Electronic Supplementary Material (ESI) for Physical Chemistry Chemical Physics.

Supplemental Material:

CH_4 dissociation on Ni(111): A quantum dynamics study of lattice thermal motion

X.J. Shen, Zhaojun Zhang and Dong H. Zhang*[1]

[1]*State Key Laboratory of Molecular Reaction Dynamics and Center for Theoretical Computational Chemistry, Dalian Institute of Chemical Physics, Chinese Academy of Sciences, Dalian, P.R. China 116023*

(Dated: May 4, 2015)

COMPUTATIONAL DETAILS

Electronic structure calculations

For ground state (GS) CH_4 dissociative adsorption on the fixed top atom of a static distorted Ni(111) surface, all *ab initio* energy calculations were carried out based on density functional theory (DFT) within the framework of the VASP(Vienna *ab initio* simulation packages) code [1, 2] which use a plane wave basis set for the electronic orbitals. The electronic exchange and correlation is described within the generalized gradient approximation using the Perdew-Wang (PW91) one [3]. The interaction of the valence electrons with the ionic cores was treated within the ultrasoft pseudopotentials (USPP) [4]. A suppercell of the Ni(111) surface has been modeled by a four layers slab and a (2×2) unit cell with a vacuum space between consecutive slabs corresponding to six metal atomic layers. A Monkhorst-Pack grid [5] of $3 \times 3 \times 1$ $\boldsymbol{k}$-points was used. The cut-off energy employed was 380 eV. An electronic smearing was introduced within the Methfessel-Paxton scheme [6] with $N = 1$ and σ=0.1 eV. Spin-polarized effect was also taken into account. The reference interaction energy (ΔV=0 eV) was referred to that configuration of the equilibrium CH_4 placing 6.0 Åabove the equilibrium rigid Ni(111) slab, unless otherwise specified.

For searching out all the transition states(TSs) of CH_4 interacting on a static distorted Ni(111) surface with a fixed Q value, the nudged elastic band method (NEB) [7–9] was used with 8 intermediate images along the reaction pathway. Such calculation was converged when the minimum force for each image was less than 0.01 eV/Å. After this first optimization, the structure of that image with the highest potential energy along the minimum energy pathway (MEP) was used as an input structure for the precise determination of the TS by minimizing all the residual forces until to the convergence criterion of 0.01 eV/Å within a quasi-Newton method.

Neutral Network(NN)

Neutral network has been succeeded in fitting the complex PES in our group for the gas molecular reactions and simple gas-surface interactions [10–13]. To fit a PES from a given set of molecular configurations, we employed the feed forward NN with two hidden layers connecting the input layer and output layer, denoted as *I*–*J*–*K*–1 NN. It has I nodes in the input layer, which equals to the number of degrees of freedom or atomic distances employed here as input coordinates for a molecular configuration, and one node in the output layer corresponding to the potential energy value of the input configuration. The two hidden layers have J and K neurons, respectively. The output of j^{th} neuron in the first hidden layer is

$$y_j^1 = f^1\Big(b_j^1 + \sum_{i=1}^{I}(w_{j,i}^1 \times x_i)\Big), \quad j = 1, 2, \cdots, J \tag{SI.1}$$

and the output of k^{th} neuron in the second hidden layer is

$$y_k^2 = f^2\Big(b_k^2 + \sum_{j=1}^{J}(w_{k,j}^2 \times y_j^1)\Big), \quad k = 1, 2, \cdots, K \tag{SI.2}$$

and consequently the final output is given by

$$y = b_1^3 + \sum_{k=1}^{K} (w_{1,k}^3 \times y_k^2), \tag{SI.3}$$

where $x_i (i = 1, \cdots, I)$ are the atomic distances for a molecular configuration, the weights $w_{j,i}^l$ connect the i^{th} neuron of $(l-1)^{th}$ layer and the j^{th} neuron of l^{th} layer, and the biases b_j^l determine the threshold of the j^{th} neuron of l^{th} layer, f^1 and f^2 are transfer functions taken as hyperbolic tangent functions. In the present study of CH_4/Ni(111) system, atomic distances as the input coordinates are the bond lengths of CH_4 and those distances between each atom of CH_4 and three high symmetric surface impact sites(fcc, hcp and atop). Additional input coordinate is considered of the degree of freedom(DOF) Q of Ni lattice. The bond lengths of CH_4 are those R_{CH1}, R_{CH2}, R_{CH3}, R_{CH4}, R_{H1H2}, R_{H1H3}, R_{H1H4}, R_{H2H3}, R_{H2H4}, R_{H3H4} satisfied the ordering of $\mathrm{R_{CH1}} \leq \mathrm{R_{CH2}} \leq \mathrm{R_{CH3}} \leq \mathrm{R_{CH4}}$. In total, there are twenty-six atomic distances as the input coordinates.

Fitting procedure

As introduced the framework of the NN method , the quality of one NN fitting strongly depends on the number of neurons for two hidden layers, i.e., the number of weights and biases used in NN fitting. For a given set of configurations, the optimum values for the weights and biases were updated by using the Levenberg-Marquardt non-linear least square algorithm [14]. The root mean square error (RMSE)function is given as

$$\mathrm{RMSE} = \sqrt{\frac{1}{n} \sum_{i=1}^{n} w_i * (E_{\mathrm{NN}} - E_{\mathrm{DFT}})^2} \tag{SI.4}$$

where $\mathrm{E_{NN}}$ and $\mathrm{E_{DFT}}$ are the energies from the evaluation of NN training and the DFT calculations. **n** is the number of configurations in the database. The RMSE is used to appraise the performance of the NN training. Moreover, we employed the "early stopping" method[15] to improve the fitting quality by dividing the entire data set into the training set and the validation set, and stopping the training procedure once over fitting occurs. It is wisdom to consider a given weighting for each term of the sum denoted by w_i in Eq. 4. In the present work, the weighting of each configuration was considered through its interaction potential energy (i.e.,E_{DFT})

$$w_i = \begin{cases} 1.0 & \mathrm{E_{DFT}} \leq 3.3 \\ 0.2 & \mathrm{E_{DFT}} \geq 3.5 \\ 0.2 + 0.4 * (1.0 + \cos\frac{(\mathrm{E_{DFT}} - 3.3)\pi}{0.2} & \text{others} \end{cases} \tag{SI.5}$$

According to this formula it is seen that we take all the configurations into account in the fitting but the small distributions for those configurations with strong repulsive potentials. Starting with a set of initial random values for the weights and biases, we perform the NN training until the RMSE of a fitting become smaller than an acceptable value. And then we carry out quantum dynamics calculations to check the final convergence of the PES. For every fitting procedure, we save two PESs with least RMSE and then do one refitting procedure

through using them as the initial sets for the weights and biases until no changes of these two PESs. When the dynamical results on these PESs also agree to each other well, even to the results from the PESs fitted with fewer points, we can believe the PES has converged for the training and stop the training procedure. Otherwise, we should select some new additional configurations from molecular dynamics simulations, perform DFT calculations with the given structures, and carry out NN training again with these additional new energy points, and then continue quantum dynamics calculations.

The Levenberg-Marquardt algorithm we adopted for NN fitting is an iteratively fitting procedure with high computational cost. The iteration time grows rapidly with respect to the size of fitting samples and network parameters. In order to accelerate the NN fitting procedure, we divided the energy points into two main parts according to the height of the carbon atom(Z_C) above the surface (i.e., entrance region and interaction region), trained and tested these two parts separately to obtain desired performances. These two segmental parts will be finally connected with a smooth window function to yield a global PES. Thus, we calculate the interaction poential energy as

$$E = f(\mathrm{Z_C}) \times \mathrm{V_{entrance}} + (1 - \mathrm{f(Z_C)}) \times \mathrm{V_{interaction}}, \tag{SI.6}$$

where the window function $\mathrm{f}(Z_C)$ with

$$f(Z_C) = \begin{cases} 0.0 & \mathrm{Z_C} \leq 2.40\text{Å} \\ 1.0 & \mathrm{Z_C} \geq 2.45\text{Å} \\ 0.5 * (1.0 - \cos\frac{(\mathrm{Z_C} - 2.40)\pi}{0.05}) & \text{others} \end{cases} \tag{SI.7}$$

In addition, we also perform NN fitting of all the energy points to obtain a global PES and compare the PESs constructed using these two different strategies. The division of the PES into two main parts can substantially reduce the coordinate space for each part, and make it feasible to reach the desired RMSE with less number of neurons. Such approach not only speeds up the training procedure, but also gives us the flexibility to put more efforts and/or more DFT energy points in a region of especial importance to dynamics.

We used a 26-60-60-1 NN structure to separately fit our database ($\sim 10^5$) consisted of two parts and finally obtained the one PESs with least RMSE values. For the entrance region part, the obtained RMSE values is only 5.4 meV, while for the interaction region part, the obtained RMSE values is 14.4 meV. Meanwhile, we do a NN training with fewer points (about 70,000) and obtain the closed RMSE values.

8D quantum model Hamiltonian and basis functions

The eight-dimensional (8D) quantum model Hamiltonian for the $XYCZ_3$ system in the Jacobi coordinates $(R, r, s, \chi, \theta_1, \varphi_1, \theta_2, \varphi_2)$ shown in Fig. 1 can be written as

$$\begin{aligned} \hat{H} = &- \frac{1}{2\mu_R}\frac{\partial^2}{\partial R^2} - \frac{1}{2\mu_r}\frac{\partial^2}{\partial r^2} + \frac{\hat{l}^2}{2\mu_r r^2} + \hat{K}^{\mathrm{vib}}_{\mathrm{CH_3}} \\ &+ \hat{K}^{\mathrm{rot}}_{\mathrm{CH_3}} + V(R, r, s, \chi, \theta_1, \varphi_1, \theta_2, \varphi_2) \end{aligned} \tag{SI.8}$$

where μ_R and μ_r are the mass of CH_4 and reduced mass of H-CH_3, R is the distance from the center of mass of CH_4 to the surface, r is the distance from the center of mass of CH_3 to

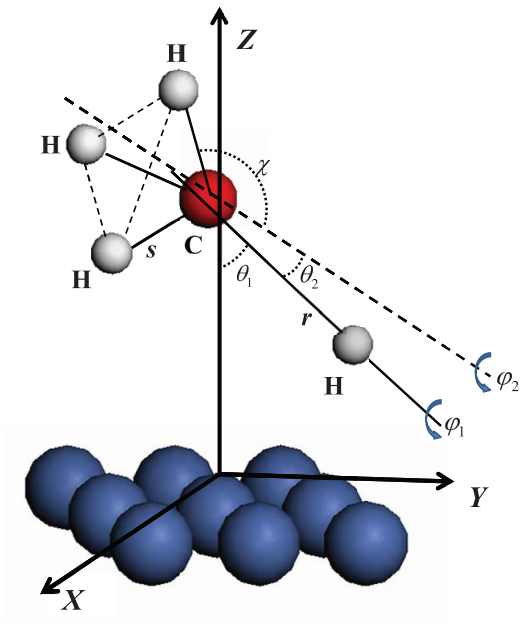

FIG. SI 1. The eight-dimensional Jacobi coordinates for the X+YCZ$_3$ system. Z and Y represent H atoms, and X represents the fixed top Ni atom of a static distorted Ni (111) surface.

H, s is the bond length of CH bond in CH_3, χ is the angle between a CH bond and the C_{3v} symmetry axis of CH_3. In this work, we have fixed the CH bond length in the CH_3 group because it almost does not change in all the TS geometries [16]. We define the bending angle between vectors R and r to be θ_1; φ_1 is the azimuth angle of the rotation of HCH_3 around the vector r; θ_2 is the bending angle between vectors r and s; φ_2 is the azimuth angle of the rotation of CH_3 around the vector s. The first two terms in Eq. SI.8 are the kinetic energy operators for R and r, respectively, and $\hat{l}$ is the orbital angular momentum operator of atom H with respect to CH_3. $\hat{K}^{\rm vib}_{\rm CH_3}$ and $\hat{K}^{\rm rot}_{\rm CH_3}$ are the vibrational and rotational kinetic energy operators of CH_3, respectively.

No vibration-rotation coupling exists due to the symmetry requirement and the definition of the CH_3-fixed frame. Because CH_3 is a symmetric top rotor, $\hat{K}^{rot}_{\rm CH_3}$ is given by

$$\hat{K}^{rot}_{\rm CH_3} = \frac{1}{2I_A}\hat{j}^2 + (\frac{1}{2I_C} - \frac{1}{2I_A})\hat{j}_z^2, \tag{SI.9}$$

where $\hat{j}^2$ is the angular monetum operator of CH_3, and $\hat{j}_z^2$ is the projection of $\hat{j}^2$ on the C_{3v} symmetry axis of CH_3, I_A and I_C are rotational inertia of CH_3, defined as

$$I_A = \frac{3}{2}m_H s^2(\sin^2\chi + \frac{2m_c}{m_c+3m_H}\cos^2\chi), \tag{SI.10}$$

and

$$I_C = 3m_H s^2 \sin^2\chi. \tag{SI.11}$$

The sticking probability, S_0, is obtained at a dividing surface placed as r=1.85 Å using a flux formalism. An L-shaped expansion for R and r was used to reduce the size of the basis set. A total of 300 sine bais functions ranging from 3.0 to 10.0 Bohr were used for the R basis set expansion with 130 nodes in the interaction region; and 6 and 30 basis

functions of r were used in the asymptotic and interaction regions, respectively. For the vibration of CH_3 group, 5 basis functions is given. The size of the rotational basis functions is controlled by the parameters, J_{max}=51, l_{max}=30, j_{max}=21 and k_{max}=3. Both OpenMP and MPI parallelization were used to render the computational costs manageable.

[1] G. Kresse and J. Furthmüller, Comput. Mater. Sci. **6**, 15 (1996).
[2] G. Kresse and J. Furthmüller, Phys. Rev. B **54**, 11169 (1996).
[3] J. P. Perdew and Y. Wang, Phys. Rev. B **45**, 13244 (1992).
[4] D. Vanderbilt, Phys. Rev. B **41**, 7892 (1990).
[5] H. J. Monkhorst and J. D. Pack, Phys. Rev. B **13**, 5188 (1976).
[6] M. Methfessel and A. T. Paxton, Phys. Rev. B **40**, 3616 (1989).
[7] G. Mills and H. Jónsson, Phys. Rev. Lett. **72**, 1124 (1994).
[8] G. Mills, H. Jónsson, and G. K. Schenter, Surf. Sci. **324**, 305 (1995).
[9] H. Jónsson, G. Mills, and K. W. Jacobsen, *in Classical and Quantum Dynamics in Condensed Phase Simulations, edited by B. J. Berne and G. Ciccotti and D. F. Coker* (World Scientific, Singapore, 1998) p. 385.
[10] J. Chen, X. Xu, X. Xu, and D. H. Zhang, J. Chem. Phys. **138**, 221104 (2013).
[11] J. Chen, X. Xu, X. Xu, and D. H. Zhang, J. Chem. Phys. **138**, 154301 (2013).
[12] T. Liu, B. Fu, and D. H.Zhang, J. Chem. Phys. **139**, 184705 (2013).
[13] B. Jiang and H. Guo, J. Chem. Phys. **141**, 034109 (2014).
[14] M. T. Hagan and M. B. Menhaj, IEEE Trans. Neural Netw. **5**, 989 (1994).
[15] W. Sarle, in *Proceedings of the 27th Symposium on the Interface of Computing Science and Statistics*, p. 352.
[16] S. Nave and B. Jackson, J. Chem. Phys. **130**, 054701 (2009).